2026 IEEE International Conference on Robotics and Automation (ICRA 2026)
June 1-5, 2026. Vienna, Austria

SureGrip: Perceptual Grasping of Natural Handholds for Free-Climbing Robots

Peter Panorel[1], Khoon Chuan Goh[1], and Kenji Nagaoka[1]

***Abstract*— Exploration of steep and irregular terrains, such as lunar caves and vertical rock faces, requires free-climbing robots capable of identifying and securely grasping natural handholds. This study introduced SureGrip, a novel framework for detecting handholds and evaluating grasp quality in free-climbing robots. By integrating depth-based contour extraction with gripper-specific contact analysis, SureGrip accurately identifies candidate handholds and quantifies their suitability using the proposed grasp metrics. Experimental results confirm that the framework can reliably detect handhold locations, estimate surface slopes, and distinguish between secure and unsuitable grasps across a range of artificial and natural surfaces. The findings emphasize the importance of both the number and placement of spine fingers for stable attachment. SureGrip thus enables informed handhold selection, improving climbing safety and efficiency.**

I. Introduction

In 2009, the Japanese lunar orbiter SELENE (SELenological and ENgineering Explorer) discovered a vertical shaft in the Marius Hills region of the Moon [1]. This feature is believed to be a skylight leading into a subsurface lava tube. The discovery sparked significant scientific interest in exploring lunar caves and skylights as potential sites for future scientific research and even human habitation [2]. However, such environments pose major mobility challenges due to irregular terrains, steep slopes, fractured rock faces, and limited accessibility. Conventional exploration systems, such as wheeled and tracked rovers, are incapable of traversing vertical or overhanging surfaces. To address these limitations, free-climbing robots [3], [7], which exploit natural handholds, have emerged as a promising alternative, offering enhanced mobility and adaptability in extreme environments.

Free-climbing robots draw inspiration from biological climbers such as geckos [8], [9], insects [10], and mammals [11] to maintain secure attachment on irregular surfaces as shown in Fig. 1. By exploiting natural features including cracks, ledges, and protrusions, these robots can significantly expand the accessible workspace of planetary exploration missions. However, their operational success critically depends on the ability to evaluate whether a surface region can safely sustain load-bearing contact under the mechanical constraints of the robot's gripper. Unlike traditional robotic manipulation scenarios that focus on grasping discrete objects, climbing robots interact with continuous, unstructured terrain where no clear object boundaries exist. The challenge is therefore not merely to detect grasp poses, but to determine whether a portion of a surface is mechanically feasible for stable attachment.

Fig. 1. Limbed climbing robot scaling an unstructured terrain [6].

Most prior work in robotic grasping has addressed object-centric grasp detection, where the objective is to estimate a stable grasp configuration for rigid, bounded objects. In contrast, climbing robots require contact feasibility assessment on continuous surfaces. The fundamental problem becomes one of mapping local surface geometry to contact mechanics conditions, specifically evaluating whether a region can support sustained forces, resist slip, and remain stable under gravitational and dynamic disturbances. This shift from object grasping to surface-based contact evaluation represents a distinct problem formulation that integrates perception with load-bearing feasibility analysis.

In this study, we present SureGrip, a gripper-aware surface feasibility estimation framework designed to enhance grasp reliability for free-climbing robots operating in terrestrial and

[1]Peter Panorel, Khoon Chuan Goh, and Kenji Nagaoka are with Department of Mechanical Engineering, Kyushu Institute of Technology, Kitakyushu 804-8550, Japan panorel.peter-aballe293@mail.kyutech.jp; goh.chuan-khoon331@mail.kyutech.jp; nagaoka.kenji572@mail.kyutech.jp

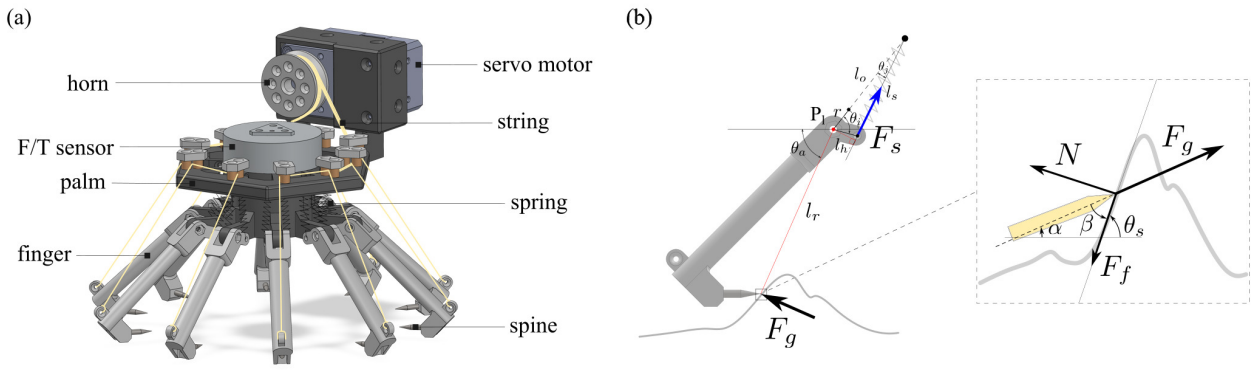

Fig. 2. Gripper design: (a) CAD model (b) Spine-surface contact model.

planetary environments. SureGrip is not a generic grasp detector; it is a gripper-aware surface feasibility estimator that evaluates whether a surface region satisfies the geometric and mechanical constraints required for stable climbing contact. Rather than predicting grasp poses for isolated objects, the framework assesses surface regions based on depth-derived geometry and quantitative grasp quality metrics grounded in contact mechanics.

The main contributions of this work are:

- Development of a depth-based surface segmentation and localization pipeline that identifies candidate contact regions on continuous, unstructured terrain without requiring prior environmental models.
- Formulation of quantitative, gripper-aware feasibility metrics that map surface geometry to load-bearing contact conditions necessary for stable grasp execution.
- Experimental validation on irregular and complex surfaces, demonstrating reliable identification and evaluation of mechanically feasible contact regions for robotic climbing.

By coupling terrain perception with gripper-specific mechanical assessment, SureGrip provides a principled framework for surface-to-contact mapping in climbing and perching applications [12]. This capability enables stable attachment under challenging conditions such as irregular surfaces, limited visibility, and communication delays typical of extraterrestrial exploration scenarios.

II. Related Works

Most research on robotic grasp detection has focused on industrial manipulators equipped with parallel-jaw grippers, primarily due to their low cost, simple structure, and widespread adoption. Existing methods can generally be categorized into two groups: 2D image–based grasping methods and 6-DOF grasping methods [13]. In 2D image–based approaches, the gripper height is typically fixed, and its orientation is constrained to be perpendicular to a single plane [14]. A large body of work within this category represents candidate grasps using oriented rectangles [15]–[20], which provide a computationally efficient abstraction of the grasp region. In contrast, 6-DOF grasping methods allow the gripper to approach the object from arbitrary orientations in three-dimensional space. However, many existing approaches are designed for known objects, where feasible grasps can be precomputed, thereby reducing the problem to one of 6D object pose estimation [21].

While effective in structured industrial settings, these approaches face significant limitations when applied to natural terrain handhold detection. Oriented rectangles, in particular, oversimplify grasp geometry by ignoring surface curvature, local slope variations, and the availability of reliable contact points, which are critical for spine-based attachment on irregular rock surfaces. Similarly, 6-DOF grasping methods often assume object priors or CAD models, which are unavailable in unstructured planetary or terrestrial environments. Moreover, both approaches are primarily designed for grasping discrete objects rather than evaluating the grippability of continuous surfaces such as cracks, ledges, or protrusions. As a result, directly transferring these techniques to natural terrain scenarios can lead to unreliable or physically infeasible handhold detection.

In addition, early studies on climbing robots relied primarily on basic image processing techniques, focusing on color and simple geometric features to identify potential handholds. For example, Tenzing utilized simplified handholds made from blue rectangular blocks, which were distinguished from background surfaces using color-based segmentation [24]. Similarly, shape detection methods were used to identify circular steel disks as handholds for a climbing robot equipped with an electromagnet end-effector [25]. However, these approaches are not directly applicable to natural terrain, where rocks often share similar color distributions with the background and exhibit highly irregular geometries.

More recent methods leverage voxelized point clouds to segment candidate handholds. Haji et al. [22] voxelized 3D point cloud data of climbing gym handholds and compared the resulting volumetric representation with the robot gripper geometry, enabling detection of graspable convex regions through geometric matching and filtering criteria. In addition, Chen et al. [23] formulated locomotion as a manipulation problem, treating movement as a sequence of grasp selection and force redistribution tasks. To determine suitable grasp

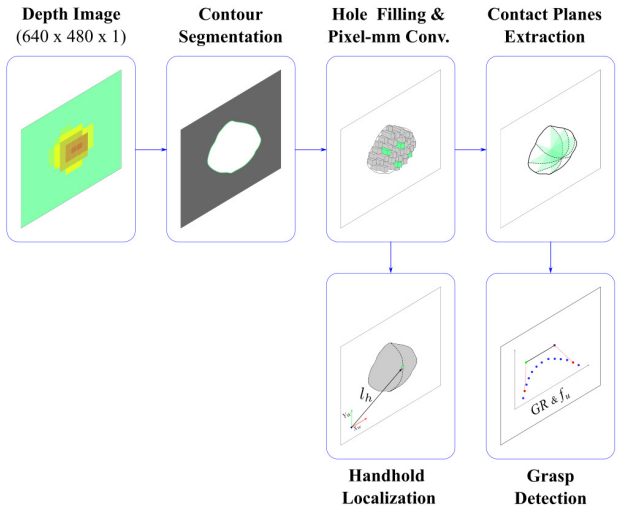

Fig. 3. The architecture of the proposed algorithm.

candidates, their system employs a coarse-to-fine perception pipeline. In the far-field stage, the captured point cloud is voxelized to obtain a structured volumetric representation of the terrain, allowing efficient extraction of locally convex surface features as potential anchor points. In the near-field stage, higher-resolution sensing refines these candidates, and each site is evaluated using a contact model that approximates the surface locally as a spherical patch. The gripper was modeled as a symmetric three-finger mechanism with two links per finger to estimate pull-force distribution under specified loading directions. Motion planning then selects feasible anchor points and optimizes boom placement and load distribution to maintain stability under tension constraints.

Nevertheless, voxel-based representations introduce discretization errors: small asperities and sharp edges may disappear due to spatial quantization, reducing geometric fidelity and potentially degrading grasp accuracy. Although decreasing voxel size improves resolution, it significantly increases computational cost and memory requirements.

These limitations highlight the need for a more robust framework for detecting and evaluating handholds on irregular, continuous surfaces. The present study addresses this gap by developing a depth-based perception and grasp detection system that provides reliable evaluation metrics tailored for free-climbing robots operating in natural environments.

III. System Overview

A. Gripper Design

Fig. 2(a) shows the design of the gripper used in this study. The gripper employs a passive spine gripper (PSG) design, in which two springs are installed for each finger to provide adhesion to the terrain during grasping. The gripper consists of seven main components: spine fingers, spine, palm, springs, string, horn, and servo motor. Ten spine fingers are arranged radially around the central part of the palm. The PSG operates with a simple mechanism: during opening, the servo motor rotates counterclockwise; once the gripper is placed against a surface, the servo motor rotates back, allowing the spine fingers to engage with the surface. The gripping force (F_g) is expressed in (1), where n is the number of springs, k is the spring stiffness, l_s and l_o are the stretched and unstretched lengths of the spring, respectively, l_h is the lever arm of the spring force (F_s), and l_r is the length from pivot point (P_l) to the spine tip.

$$F_g = \frac{nk(l_s - l_o)l_h}{l_r} \tag{1}$$

Fig. 2(b) illustrates the spine–surface contact model. In this model, force equilibrium is governed by the following conditions:

$$F_g \sin\beta = N \tag{2}$$

$$F_g \cos\beta \leq \mu_s N \tag{3}$$

$$\theta_s \leq \alpha + \tan^{-1}\left(\frac{1}{\mu_s}\right). \tag{4}$$

Here, α denotes the angle between F_g and the horizontal plane, while μ_s is the coefficient of static friction between the spine and the surface. Equation (4) indicates that, for a gripper with a fixed spine angle and a given terrain, there exists a minimum surface slope ($\theta_{s_{\min}}$) at which a spine can achieve stable attachment.

B. Algorithm Pipeline

This paper proposes SureGrip, a framework that generates pixel-level grasp predictions from depth images. The pipeline consist of six modules, as illustrated in Fig. 3. Depth images ($D \in \mathbb{R}^{H\times W}$) are captured using an Intel RealSense D435i camera at a resolution of 640 × 480 pixels and a frame rate of 30 frames per second (fps). In natural terrains, handholds often appear as clusters that protrude from surrounding surfaces or walls. To extract these candidate regions, contour segmentation is applied. First, the wall depth (d_w) is estimated as the mode of the depth measurements, representing the dominant planar surface. A binary mask (B) is then generated from the depth image to define points closer than the wall, defined as:

$$B(i,j) = \mathbf{1}\big[d(i,j) \leq d_w\big]. \tag{5}$$

Noise in the binary mask is removed using a 5×5 median filter, followed by a closing morphological operation with a 9×9 kernel. The outer boundaries of each detected contour are then extracted and stored into an array:

$$H = [h_1, h_2, ..., h_n], h \in \mathbb{R}^{M\times N}, \tag{6}$$

where $M \times N$ denotes the spatial dimensions of each handhold patch.

Since missing depth information is an inherent limitation of depth cameras [26], [27], gaps in the data are filled via linear interpolation between neighboring valid pixels. Each handhold's image coordinates are subsequently mapped

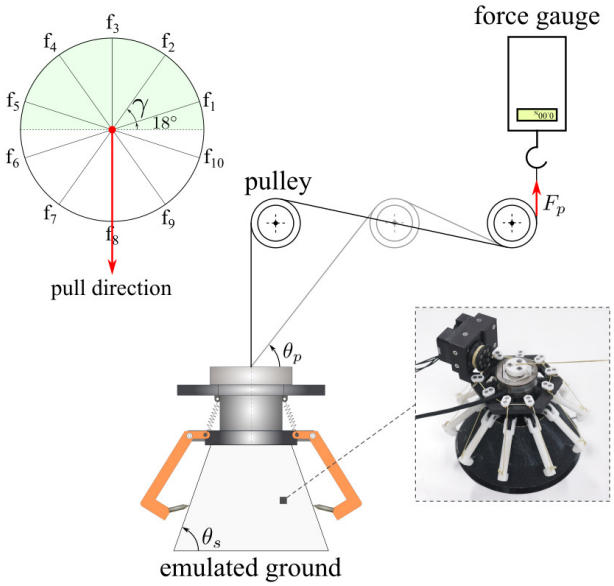

Fig. 4. Experimental set-up for grasping tests.

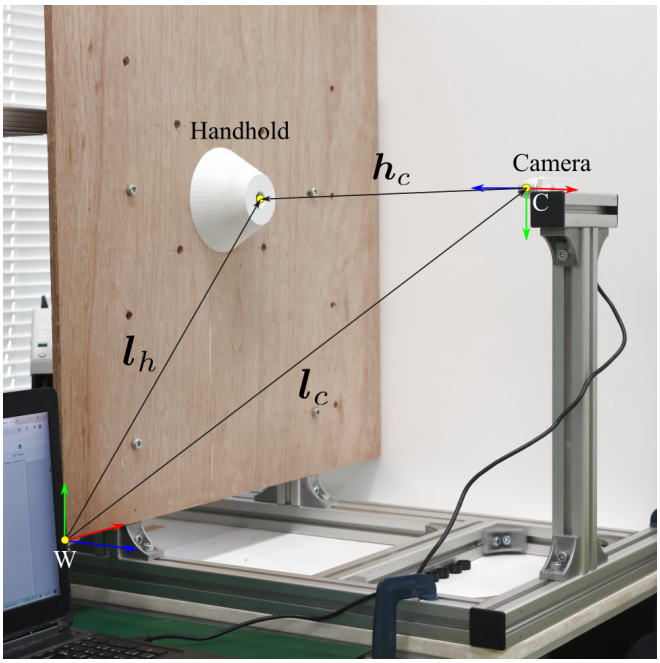

Fig. 5. Experimental set-up for handhold detection tests.

to the camera coordinate system using the pinhole camera model:

$$x_c = \frac{(i - O_x)z_c}{f_x} \tag{7}$$

$$y_c = \frac{(j - O_y)z_c}{f_y} \tag{8}$$

where (O_x,O_y) and (f_x,f_y) denote the camera's principal point and focal lengths, respectively.

After coordinate conversion, the pipeline branches into two modules: handhold localization and grasp detection. In the localization branch, the centroid (c_x, c_y) of each handhold is computed by averaging its transformed coordinates. In the grasp detection branch, contact planes between the gripper and terrain are extracted. Points along lines passing through (c_x, c_y) are sampled at angles of $\lambda = 45°$, as illustrated in Fig. 4, with row and column indices given by:

$$\left.\begin{aligned} i &= c_x + t\cos\lambda \\ j &= c_y + t\sin\lambda \end{aligned}\right\} t \in \left[-\frac{\min(M,N)}{2}, \frac{\min(M,N)}{2}\right]. \tag{9}$$

Finally, grasp quality is evaluated by fitting the gripper geometry to the cross-sections of each contact plane. The resulting metrics, described in the following section, quantify the suitability of individual handholds for successful grasp execution by the selected spine gripper. Once a handhold is determined to be suitable and its position is known, the robot can plan and execute a grasp by using inverse kinematics to align the gripper perpendicular to the handhold, enabling secure attachment during climbing maneuvers.

IV. Experiments

A. Grasping Tests

Grasping tests were conducted to determine the minimum surface slope required for stable attachment ($\theta_{s_{\min}}$) and to evaluate the influence of finger combinations on the pulling force (F_p), where F_p denotes the maximum force the gripper can sustain before detachment. Fig. 4 illustrates the experimental setup. A #40 sandpaper layer was attached to a truncated conical surface to approximate rough terrain contact. The conical geometry was selected to provide a controlled and continuous slope distribution, enabling systematic evaluation of the relationship between surface inclination and pulling force under repeatable conditions.

The gripper was placed on the cone and pulled until detachment. Pulling was performed at angles ranging from 0° to 90° in 30° increments, and the corresponding pulling force was measured using a digital force gauge. This procedure was repeated for cone inclinations of 50°, 60°, and 70°. The cone had a height of 61 mm and a base diameter of 135 mm. Each pulling configuration was tested four times.

To quantify grasp suitability from depth measurements, a parameter termed Grasp Rating (GR) is introduced. GR is defined as the ratio of the number of fingers (n_f) in contact with the surface that satisfy $\theta_s \geq \theta_{s_{\min}}$ to the total number of fingers (n_t), as expressed in (10):

$$\text{GR} = \frac{n_f}{n_t}. \tag{10}$$

In addition to contact count, spatial distribution of the fingers is considered. For a downward pulling direction, the gripper is conceptually divided into upper and lower halves, with the upper half highlighted in Fig. 4. The number and arrangement of engaged fingers are systematically varied to identify configurations that promote stable attachment.

B. Detection and Localization Tests

Fig. 5 shows the experimental setup used during testing. An Intel RealSense D435i camera was placed at the initial

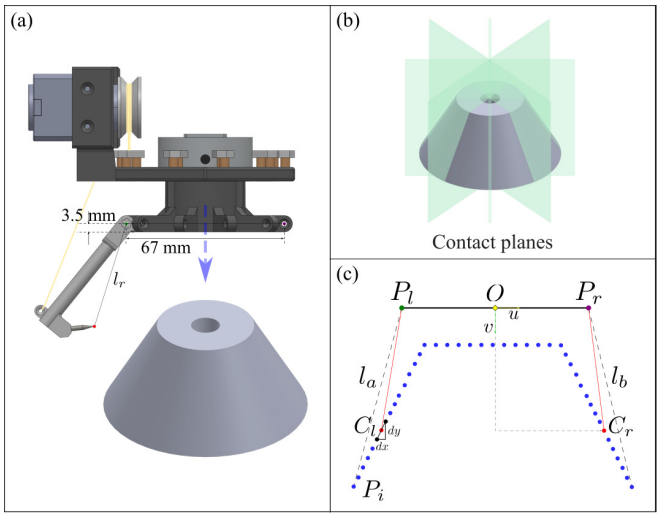

Fig. 6. Gripper point contact.

location ($\boldsymbol{l}_c$), and the proposed algorithm was then executed to detect all available handholds within the camera frame. The positions of these handholds ($\boldsymbol{l}_h$) were computed relative to the world frame ($\boldsymbol{W}$) using (11). Here, R_c denotes the rotation matrix representing the camera orientation, and $\boldsymbol{h}_c$ represents the handhold coordinates in the camera frame.

$$\boldsymbol{l}_h = \boldsymbol{l}_c + R_c \boldsymbol{h}_c \tag{11}$$

C. Slope Detection Tests

To determine grippable handhold candidates, the surface inclination at the point of interaction between spine and surface was calculated. Fig. 6 illustrates the components involved in contact point calculation. The test was conducted using a 3D-printed truncated cone with a 60° inclination. First, the depth map was divided into five planes corresponding to the contact locations of the ten spine fingers, as shown in Fig. 6(b). Next, the geometry of the gripper was aligned with the cross-sections (blue dots) within these planes (Fig. 6(c)). The gripper center was positioned above the centroid of the contour, with an offset of 3.5 mm from the highest point of the contour to match the gripper geometry. The points P_l and P_r represent the left and right pivot points of two opposing fingers. The contact points for the left and right fingers, C_l and C_r, were then obtained using the following relations:

$$l_a = \left\| P_l - \sum_{i=1}^{k} P_i \right\|, \qquad C_l = P_i \quad \text{if } |l_r - l_a| \leq \text{tol} \tag{12}$$

$$l_b = \left\| P_r - \sum_{i=1}^{k} P_i \right\|, \qquad C_r = P_i \quad \text{if } |l_r - l_b| \leq \text{tol} \tag{13}$$

Each contour point (P_i) was compared with the reference points P_l and P_r. If the distance between them fell within a specified tolerance, the point is identified as a contact point (C_l or C_r), as shown by the red dots in Fig. 6(c). The coordinates of each contact point, $C = (u, v)$, were expressed relative to the center of the gripper O. To determine the surface inclination at the contact, two neighboring points were sampled on either side of C_l and C_r, and the corresponding local slope was computed to assess whether the contour qualified as a candidate handhold.

TABLE I

AVERAGE PULLING FORCE (F_p) AT DIFFERENT SURFACE INCLINATIONS (θ_s).

$\boldsymbol{\theta_s}$ [°]	**Ave. Pulling Force** [N]			
	$\boldsymbol{\theta_p} = 0°$	30°	60°	90°
50	5.35	7.83	8.40	10.73
60	11.75	15.15	23.20	17.75
70	20.75	24.10	33.13	47.78

D. Algorithm Evaluation Tests

Finally, the proposed algorithm was evaluated on a range of objects, including both artificial samples and natural terrain. The gripper was oriented such that finger f_1 was positioned 18° from the horizontal (Fig. 4), with the candidate upper fingers defined as $[f_1, f_2, f_3, f_4, f_5]$. Three representative test samples were considered: a 50° cone, a polyurethane (PU) climbing hold, and a limestone rock. For each case, the algorithm assessed the object's suitability as a candidate handhold by computing GR and the number of upper fingers that satisfied the slope criterion (f_u). To further validate the predictions, physical grasping tests were also conducted, confirming the reliability of the algorithm in real-world conditions.

V. Results and Discussion

A. Grasping Test Results

Table I presents the experimental results of the grasping tests conducted at various surface inclinations. The results show that the pulling force (F_p) increases with surface slope, indicating that steeper surfaces support higher load capacity. In addition, F_p decreases as the pulling angle is reduced from 90° to 0°, with the lowest resistance occurring at 0°.

The minimum surface inclination ($\theta_{s_{\min}}$) was determined based on the payload requirement of the climbing platform. For this study, calculations were performed for XCLIMBER [6], a prototype quadruped free-climbing robot with a mass of 5.5 kg operating under lunar gravity. During locomotion, at least three limbs must support the entire body weight. Static equilibrium analysis indicates that each gripper must therefore provide a minimum pulling force ($F_{p_{\min}}$) of 3 N.

From Table I, considering the pulling angle of 0° which produces the lowest measured F_p, a $\theta_{s_{\min}}$ of 60° was selected. At this inclination, the gripper provides $F_p = 11.75$ N, which is approximately 3.9 times greater than $F_{p_{\min}}$. This margin provides robustness against disturbances and modeling uncertainties during climbing. Accordingly, handholds with local surface inclinations greater than or equal to 60° are classified as suitable for secure attachment.

In natural terrain, surface inclinations vary locally and spine engagement occurs across multiple orientations. To

TABLE II

AVERAGE PULLING FORCE (F_p) AT DIFFERENT FINGER COMBINATIONS.

No.	**Finger Combination** (FC)	**Finger count** (n_f)	**Upper finger count** (n_u)	**Grasp Rating** (GR)	**Ave. Pulling Force** [N]
1	f_2, f_3, f_4	3	3	0.3	6.43
2	f_1, f_2, f_5, f_6	4	3	0.4	8.10
3	f_2, f_3, f_4, f_5	4	4	0.4	9.75
4	$f_6, f_7, f_8, f_9, f_{10}$	5	0	0.5	5.58
5	f_1, f_2, f_4, f_5, f_6	5	4	0.5	11.35
6	f_1, f_2, f_3, f_4, f_5	5	5	0.5	11.40
7	$f_1, f_6, f_7, f_8, f_9, f_{10}$	6	1	0.6	5.90
8	$f_1, f_2, f_4, f_5, f_6, f_{10}$	6	4	0.6	10.73
9	$f_1, f_5, f_6, f_7, f_8, f_9, f_{10}$	7	2	0.7	8.48
10	$f_1, f_2, f_5, f_6, f_7, f_8, f_9, f_{10}$	8	3	0.8	9.20
11	$f_1, f_2, f_3, f_4, f_5, f_6, f_7, f_8, f_9, f_{10}$	10	5	1.0	11.75

evaluate the influence of finger participation and spatial distribution on pulling performance, eleven finger combinations based on the orientations shown in Fig. 4 were tested on a 60° conical surface. The results are summarized in Table II.

As the number of engaged fingers decreases from 10 to 3, the pulling force drops significantly from 11.75 N to 3 N, confirming that distributed engagement increases load-bearing capacity. However, total finger count alone does not determine performance. For example, FC7 ($n_f = 6$) produces a lower pulling force (5.9 N) than FC1 ($n_f = 3$, 6.43 N). The distinguishing factor is the number of upper-half fingers: FC1 has $f_u = 3$, whereas FC7 has only $f_u = 1$. Fingers located in the upper half play a dominant role in resisting overturning moments during downward pulling, consistent with [5].

These results demonstrate that both engagement quantity and spatial distribution govern grasp stability. Accordingly, a suitable handhold candidate is defined by GR ≥ 0.4 and $f_u \geq 2$, ensuring sufficient contact redundancy and effective moment resistance. The experimental trends therefore provide a mechanical interpretation of the suitability metrics: the slope threshold enforces hook-based interlocking, while GR and f_u promote distributed load sharing that improves stability. This establishes a direct link between the geometric evaluation criteria and the measured load-bearing behavior of the spine gripper.

It should be noted that the conical surface provides a controlled and continuous slope distribution, enabling systematic isolation of the relationship between surface inclination, finger engagement, and pulling force. Although this geometry does not replicate the full irregular morphology of natural rock, it allows the minimum slope threshold and engagement criteria to be validated under repeatable conditions. The natural terrain experiments extend this validation to nonuniform surfaces; however, broader terrain variability and large-scale field validation remain subjects for future work. Therefore, the proposed geometric suitability metrics should be interpreted as local engagement criteria rather than a complete representation of all natural rock interactions.

B. Detection and Localization Results

Fig. 7 shows the result of the handhold detection test. The proposed algorithm successfully identifies the contours of the 4 handholds present on the wall, which are highlighted with green outlines in Fig. 7(b). Furthermore, the positions of these candidate handholds were calculated and compared with their measured values, as shown in Table III. The results indicate that the algorithm can accurately detect and localize each handhold, with position errors within ± 7.77 mm.

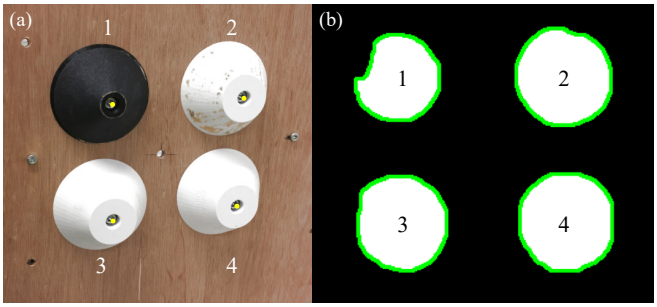

Fig. 7. Handhold detection: (a) Handholds (b) Detected contours.

C. Slope Detection Results

Table IV summarizes the results of the slope detection tests. Each of the five planes of the truncated cones has a true slope of 60°. The calculated slopes (θ_s) for the left and right fingers exhibited an average error of approximately $\pm 6.0^\circ$, although in two cases the deviation increased to about $\pm 20.0^\circ$. These larger errors are likely caused by holes in the depth measurements. Although the algorithm applies linear interpolation to fill missing data, the true values cannot be fully recovered, so these approximations can still introduce inaccuracies. Overall, the algorithm provides a close estimate of the true slope values, but performance could be further improved by reducing depth measurement gaps, for example, by adjusting the camera-to-handhold distance, since the current setup relied on a single fixed distance.

In addition, the locations of the contact points were computed, yielding an average positional error of approximately ± 2.7 mm, indicating good overall accuracy. However, in areas affected by missing depth data, the error increased to nearly ± 20 mm, which is undesirable. Despite these occasional deviations, the proposed algorithm provides reliable predictions of both contact point locations and corresponding surface inclination angles.

TABLE III

COMPARISON OF MEASURED COORDINATES WITH GROUND TRUTH AND CALCULATED DISTANCES.

Handhold No.	**Calculated** [mm]			**Ground Truth** [mm]			**Calc. Dist.** [mm]	**True Dist.** [mm]	**Error** [mm]
	X	Y	Z	X_W	Y_W	Z_W			
1	230.9	474.7	62.2	220	480	61	529.66	531.53	$\pm$1.87
2	411.6	475.5	62.2	400	480	61	630.07	627.79	$\pm$2.28
3	233.8	319.1	62.2	220	325	61	526.76	518.99	$\pm$7.77
4	413.8	321.8	62.2	400	325	61	400.72	397.17	$\pm$3.55

TABLE IV

SLOPE CALCULATION RESULTS.

Plane	**Calc. Pos.** [mm]				**CAD Values** [mm]			**Calc. Dist.** [mm]		**True Dist.** [mm]	**Calc. Slope** [°]		**True Slope** [°]	**Pos. Error** [mm]		**Slope Error** [°]	
	u_l	v_l	u_r	v_r	u_l	u_r	v	L	R	L=R	L	R	L=R	L	R	L	R
1	-53.16	38.29	58.59	35.21	-53.9	53.9	40.94	65.51	68.36	67.69	68.5	53.0	60	$\pm$2.17	$\pm$0.67	$\pm$8.5	$\pm$7.0
2	-53.78	38.01	57.04	36.24	-53.9	53.9	40.94	65.86	67.58	67.69	65.4	56.8	60	$\pm$1.83	$\pm$0.11	$\pm$5.4	$\pm$3.2
3	-55.34	37.14	50.63	39.30	-53.9	53.9	40.94	66.65	64.09	67.69	57.6	82.0	60	$\pm$1.04	$\pm$3.59	$\pm$2.4	$\pm$22
4	-21.86	41.25	17.11	39.73	-53.9	53.9	40.94	46.68	43.26	67.69	69.9	80.3	60	$\pm$21.0	$\pm$24.43	$\pm$9.9	$\pm$20.3
5	-47.54	40.44	45.36	41.07	-53.9	53.9	40.94	62.41	61.19	67.69	64.9	65.2	60	$\pm$5.27	$\pm$6.49	$\pm$4.9	$\pm$5.2

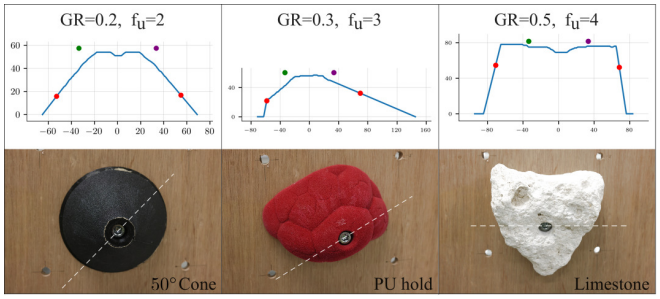

Fig. 8. Algorithm evaluation

D. Algorithm Evaluation Results

Fig. 8 presents the test samples along with representative contour plots from the algorithm, including the corresponding GR and f_u values. The three samples produced GR values of 0.2, 0.3, and 0.5, and f_u values of 2, 3, and 4 for the 50° cone, polyurethane climbing hold, and limestone rock, respectively. According to the criteria (GR ≥ 0.4 and $f_u \geq 2$), only the limestone sample qualifies as a suitable handhold, while the cone and climbing hold do not meet the requirements.

To verify these findings, grasping tests were carried out to measure the pulling force of the gripper on each sample. Tests were performed at a 0° pulling direction, where F_p is expected to be minimal. The measured forces were 5.35 N, 6.47 N, and 60.1 N for the cone, climbing hold, and limestone, respectively. These results closely align with the algorithm's predictions, confirming that the cone and climbing hold are unsuitable for secure grasping, whereas the limestone provides a reliable and robust handhold. This outcome demonstrates the algorithm's effectiveness in distinguishing suitable from unsuitable handholds, reinforcing its potential for robotic climbing in natural terrains.

VI. CONCLUSIONS

This paper presented SureGrip, a gripper-aware surface feasibility estimation framework developed for free-climbing robots equipped with spine grippers. Rather than treating grasping as an object-centric detection problem, SureGrip formulates climbing interaction as a contact feasibility prediction task on continuous and irregular surfaces. The framework integrates depth-based perception with gripper-specific contact mechanics analysis to evaluate whether a surface region can sustain load-bearing attachment under geometric constraints.

The proposed pipeline performs surface segmentation from depth images, localizes candidate contact regions, and evaluates their mechanical suitability using quantitative metrics derived from the geometry and force transmission characteristics of the spine gripper. In this sense, SureGrip does not merely detect handholds; it maps local surface geometry to contact feasibility conditions required for stable climbing.

Experimental validation on artificial and natural surfaces, including truncated cones, polyurethane climbing holds, and limestone rocks, demonstrated accurate localization with position errors within ±7.77 mm, reliable surface inclination estimation with an average slope error of ±6°, and strong agreement between predicted grasp quality and measured pulling forces. These results confirm that the framework effectively translates geometric perception into mechanically meaningful attachment predictions.

Although the current implementation performs deterministic feasibility evaluation, the formulation naturally extends toward uncertainty-aware contact reasoning. Future work will investigate probabilistic surface modeling, stochastic contact sampling, and Monte Carlo based evaluation of grasp robustness under geometric uncertainty. Such extensions would enable climbing feasibility prediction that explicitly accounts for sensing noise, surface variability, and friction uncertainty, further enhancing reliability in extreme and extraterrestrial environments.

Overall, SureGrip establishes a principled surface-to-contact mapping framework that supports stable climbing and perching behaviors for free-climbing and aerial robotic systems operating in challenging terrestrial and planetary settings.

ACKNOWLEDGMENT

This work was partly supported by FAIS Research and Development Project and JSPS KAKENHI Grant Number JP25K07683.

REFERENCES

[1] J. Haruyama et al., Possible lunar lava tube skylight observed by SELENE cameras, Geophysical Research Letters, vol. 36, no. 21, 2009.

[2] T. Kaku et al., Detection of intact lava tubes at Marius Hills on the Moon by SELENE (Kaguya) Lunar Radar Sounder, Geophysical Research Letters, vol. 44, no. 20, pp. 10–155, 2017.

[3] K. Uno et al., Hubrobo: a lightweight multi-limbed climbing robot for exploration in challenging terrain, in 2020 IEEE-RAS 20th International Conference on Humanoid Robots (Humanoids), IEEE, 2021, pp. 209–215.

[4] K. Nagaoka et al., Passive spine gripper for free-climbing robot in extreme terrain, IEEE Robotics and Automation Letters, vol. 3, no. 3, pp. 1765—1770, 2018.

[5] P. A. Panorel and K. Nagaoka, Development of a self-locking spine gripper for power-efficient robotic climbing in extreme terrain, Advanced Robotics, vol. 39, no. 21, 2025, pp. 1329-–1345.

[6] P. A. Panorel and K. Nagaoka, XCLIMBER: Design and development of an energy-efficient free-climbing robot with self-locking mobility for extreme terrain, Proceedings of the 8th International Conference on Advanced Mechatronics (ICAM), JSME, 2024, pp. 234-235 (#FC3-2).

[7] P. Nadan, S. Backus, A. M. Johnson, LORIS: A lightweight free-climbing robot for extreme terrain exploration, in 2024 IEEE International Conference on Robotics and Automation (ICRA), IEEE, 2024, pp. 18480—18486.

[8] O. Unver et al., Geckobot: A gecko inspired climbing robot using elastomer adhesives, In Proceedings 2006 IEEE International Conference on Robotics and Automation (ICRA), IEEE, 2006. (pp. 2329-2335).

[9] A. Parness et al., LEMUR 3: A limbed climbing robot for extreme terrain mobility in space, in 2017 IEEE International Conference on Robotics and Automation (ICRA), 2017, pp. 5467–5473.

[10] P. Zi et al., A mechanical adhesive gripper inspired by beetle claw for a rock climbing robot, Mechanism and Machine Theory, vol. 181, 2023.

[11] A. Sintov, T. Avramovich, and A. Shapiro, Design and motion planning of an autonomous climbing robot with claws, Robotics and Autonomous Systems, vol. 59, no. 11, pp. 1008–1019, 2011.

[12] W. R. Roderick, M. R. Cutkosky, and D. Lentink, Bird-inspired dynamic grasping and perching in arboreal environments, Science Robotics, vol. 6, no. 61, 2021.

[13] Z. Yin, and Y. Li, Overview of robotic grasp detection from 2D to 3D, Cognitive Robotics, vol. 2, pp. 73–82, 2022.

[14] G. Du et al., Vision-based robotic grasping from object localization, object pose estimation to grasp estimation for parallel grippers: a review, Artificial Intelligence Review, vol. 54, no. 3, pp. 1677–1734, 2021.

[15] Y. Jiang, S. Moseson, and A. Saxena, Efficient grasping from rgbd images: Learning using a new rectangle representation, in 2011 IEEE International conference on robotics and automation (ICRA), IEEE, 2011, pp. 3304–3311.

[16] I. Lenz et al., 2015, Deep learning for detecting robotic grasps, The International Journal of Robotics Research, vol. 34, no. 4–5, 2015, pp. 705–724.

[17] L. Pinto and A. Gupta, Supersizing self-supervision: Learning to grasp from 50k tries and 700 robot hours, in 2016 IEEE international conference on robotics and automation (ICRA), IEEE, 2016, pp. 3406–3413.

[18] J. Redmon and A. Angelova, Real-time grasp detection using convolutional neural networks, in 2015 IEEE international conference on robotics and automation (ICRA), IEEE, 2015, pp. 1316–1322.

[19] Q. Zhang et al., Robust robot grasp detection in multimodal fusion, MATEC Web of Conferences, EDP Sciences, vol. 139, 2017.

[20] X. Zhou et al., Fully convolutional grasp detection network with oriented anchor box, in 2018 IEEE/RSJ International Conference on Intelligent Robots and Systems (IROS), IEEE, 2018, pp. 7223–7230.

[21] C. Wang et al., Densefusion: 6d object pose estimation by iterative dense fusion, In Proceedings of the IEEE/CVF conference on computer vision and pattern recognition, 2019, pp. 3343–3352.

[22] K. Haji et al., Gripping Target Detection in Terrain Based on Geometrical Configuration of a Gripper for Free-Climbing Robots, In Proceedings of the 2020 JSME Conference on Robotics and Mechatronics, JSME, 2020, pp. 2P1–B06 (in Japanese).

[23] T., Chen et al., Locomotion as manipulation with ReachBot, Science Robotics, vol. 9, no. 89, 2024, p. eadi9762.

[24] S. P. Linder, E. Wei, and A. Clay, Robotic rock climbing using computer vision and force feedback, In Proceedings of the 2005 IEEE International Conference on Robotics and Automation (ICRA), IEEE, 2005, pp. 4685–4690.

[25] K. Albee et al., Motion planning for climbing mobility with implementation on a wall-climbing robot,In 2019 IEEE aerospace conference, IEEE, 2019, pp. 1–10.

[26] J. M. Cho, S. Y. Park, and S. I. Chien, Hole-filling of realsense depth images using a color edge map, IEEE access,vol. 8, pp. 53901–53914, 2020.

[27] S. W. Nam et al, Hole-filling methods using depth and color information for generating multiview images, ETRI Journal, vol. 38, no. 5, pp. 996–1007, 2016.